CAVIN1-Mediated hERG Dynamics

Zeina R Al Sayed, Céline Pereira, Rémi Le Borgne, Christine Viaris de Lesegno, Charlène Jouve, Esthel Pénard, Adeline Mallet, Nihar Masurkar, Gildas Loussouarn, Jean-Marc Verbavatz, et al.

Circulation

ORIGINAL RESEARCH ARTICLE

CAVIN1-Mediated hERG Dynamics: A Novel Mechanism Underlying the Interindividual Variability in Drug-Induced Long QT

Zeina R. Al Sayed, PhD; Céline Pereira, MSC; Rémi Le Borgne, MSC; Christine Viaris de Lesegno, PhD; Charlène Jouve, MSC; Esthel Pénard, MSC; Adeline Mallet, PhD; Nihar Masurkar, PhD; Gildas Loussouarn, PhD; Jean-Marc Verbavatz, PhD; Christophe Lamaze, PharmD-PhD; David-Alexandre Trégouët, PhD; Jean-Sébastien Hulot, MD-PhD

BACKGROUND: Drug-induced QT prolongation (diLQT) is a feared side effect that could expose susceptible individuals to fatal arrhythmias. The occurrence of diLQT is primarily attributed to unintended drug interactions with cardiac ion channels, notably the hERG (human ether-a-go-go-related gene) channels that generate the delayed-rectifier potassium current (I_{Kr}) and thereby regulate the late repolarization phase. There is an important interindividual susceptibility to develop diLQT, which is of unknown origin but can be reproduced in patient-specific induced pluripotent stem cell–derived cardiomyocytes (iPS-CMs). We aimed to investigate the dynamics of hERG channels in response to sotalol and to identify regulators of the susceptibility to developing diLQT.

METHODS: We measured electrophysiological activity and cellular distribution of hERG channels after hERG blocker treatment in iPS-CMs derived from patients with highest sensitivity (HS) or lowest sensitivity (LS) to sotalol administration in vivo (ie, on the basis of the measure of the maximal change in QT interval 3 hours after administration). Specific small interfering RNAs and CAVIN1-T2A-GFP adenovirus were used to manipulate *CAVIN1* expression.

RESULTS: Whereas HS and LS iPS-CMs showed similar electrophysiological characteristics at baseline, the late repolarization phase was prolonged and I_{Kr} significantly decreased after exposure of HS iPS-CMs to low sotalol concentrations. I_{Kr} reduction was caused by a rapid translocation of hERG channel from the membrane to the cytoskeleton-associated fractions upon sotalol application. *CAVIN1*, essential for caveolae biogenesis, was 2× more highly expressed in HS iPS-CMs, and its knockdown by small interfering RNA reduced their sensitivity to sotalol. *CAVIN1* overexpression in LS iPS-CMs using adenovirus showed reciprocal effects. We found that treatment with sotalol promoted translocation of the hERG channel from the plasma membrane to the cytoskeleton fractions in a process dependent on CAVIN1 (caveolae associated protein 1) expression. *CAVIN1* silencing reduced the number of caveolae at the membrane and abrogated the translocation of hERG channel in sotalol-treated HS iPS-CMs. CAVIN1 also controlled cardiomyocyte responses to other hERG blockers, such as E4031, vandetanib, and clarithromycin.

CONCLUSIONS: Our study identifies unbridled turnover of the potassium channel hERG as a mechanism supporting the interindividual susceptibility underlying diLQT development and demonstrates how this phenomenon is finely tuned by CAVIN1.

Key Words: caveolae ■ myocytes, cardiac ■ sensitivity and specificity

Interindividual variability in drug response is unpredictable and remains largely unexplained. Whereas most patients develop an appropriate drug response in terms of efficacy and safety, some patients treated with cardiac or noncardiac medications experience adverse side effects that can be life-threatening. The

Correspondence to: Jean-Sébastien Hulot, MD-PhD, PARCC, 56 Rue Leblanc, F-75015 Paris, France. Email jean-sebastien.hulot@aphp.fr
Supplemental Material is available at https://www.ahajournals.org/doi/suppl/10.1161/CIRCULATIONAHA.123.063917.
For Sources of Funding and Disclosures, see page XXX.

Circulation is available at www.ahajournals.org/journal/circ

Clinical Perspective

What Is New?

- The interindividual susceptibility underlying drug-induced QT prolongation development involves unbridled turnover of cardiac ion channels from the plasma membrane.
- This phenomenon is finely tuned by CAVIN1 (caveolae associated protein 1), a protein that is essential for caveolae biogenesis.
- Treatment with hERG (human ether-a-go-go-related gene) blocker promoted translocation of the hERG channel from the plasma membrane to the cytoskeleton-associated fractions in a process dependent on CAVIN1 expression.

What Are the Clinical Implications?

- Whereas congenital long QT syndrome arises primarily from a genetic origin, the development of drug-induced long QT syndrome involves differences in the trafficking machinery of cardiac ion channels.
- The prediction of CAVIN1 expression levels could help prevent drug-induced cardiotoxicity.

Nonstandard Abbreviations and Acronyms

AP	action potential
APD	action potential duration
BSA	bovine serum albumin
CAV1	caveolin-1
CAV3	caveolin-3
CAVIN1	caveolae associated protein 1
diLQT	drug-induced QT prolongation
DMSO	dimethyl sulfoxide
FP	field potential
FDP	field potential duration
hERG	human ether-a-go-go-related gene
HS	high sensitivity
IKr	delayed-rectifier potassium current
iPSC	induced pluripotent stem cell
iPS-CMs	induced pluripotent stem cell–derived cardiomyocytes
iQTEST	Selections of Subjects With Important Changes in Their Cardiac Repolarization Parameters for the Procurement of Skin and Blood Samples
LS	low sensitivity
LQTS	long QT syndrome
MβCD	methyl-β-cyclodextrin
MEA	multielectrode array
RPMI	Roswell Park Memorial Institute
siRNA	small interfering RNA

development of drug-induced QT prolongation (diLQT) and consequent fatal arrhythmias (ie, torsade de pointes) in some patients is one of the most striking examples of cardiotoxicity.[1] The occurrence of diLQT is primarily related to drug interactions with cardiac ion channels, notably the hERG (human ether-a-go-go-related gene) channels that regulate the late repolarization phase through the rapid component of the cardiac delayed-rectifier potassium current (I_{Kr}). This channel constitutes a common unintended target of drugs from almost every therapeutic class, including antiarrhythmic, antipsychotic, antibiotic, antihistamine, and anticancer agents.[1,2] Why some patients are more susceptible than others and display excessive inhibition of hERG channels in response to the same pharmacological stimulation is unclear.[3]

Because sequence variations in *KCNH2* (the gene encoding hERG) are detected in patients with congenital long QT syndrome (LQTS), the existence of genetic determinism to diLQT has been proposed.[4–7] However, genome-wide screening studies in large cohorts of patients with diLQT have globally ruled out the essential contribution of variants of *KCNH2* or other genes involved in congenital LQTS.[8,9]

We and others previously reported that the predilection to diLQT as observed in vivo could be reproduced in vitro using induced pluripotent stem cell–derived cardiomyocytes (iPS-CMs).[10,11] These studies suggest the in vitro reproduction of a peculiar mechanism that supports the interindividual variability in the susceptibility to develop diLQT. Here, we exploited iPS-CMs derived from individuals with differential sensitivity to sotalol,[10] a class III antiarrhythmic drug and an unintentional hERG blocker, to investigate any common molecular mechanism promoting high sensitivity to hERG blockers. By comparing the transcriptomic profiles of iPS-CMs for individuals with extreme response to sotalol, we previously identified 5 differentially expressed genes (*CAMKV*, *DLG2*, *KCNE4*, *HTR2C*, and *CAVIN1*) that were mainly related to the regulation of cardiac repolarization.[10] Our data demonstrate that *CAVIN1*, an essential gene for caveolae biogenesis, mediates diLQT. High expression levels of this gene drove hERG translocation between the plasma membrane and the cytoskeleton upon drug exposure, leading to I_{Kr} reduction and the consequent prolongation in the repolarization phase in iPS-CMs derived from individuals presenting with sotalol-induced LQTS.

METHODS

Details on the procedures are provided in the Supplemental Material. The data and material that support the findings of this study are available from the corresponding author upon reasonable request.

Induced Pluripotent Stem Cell Maintenance in Cultures

Skin biopsies from 10 individuals with the highest QT interval prolongation (high sensitivity [HS]) and 10 individuals with the lowest change in QT (low sensitivity [LS]) after sotalol administration were reprogrammed into induced pluripotent stem cells (iPSCs), as previously reported.[10] The protocol was approved by the local institutional ethics committee (CPP Ile de France XI institutional review board number 11-015; iQTEST [Selections of Subjects With Important Changes in Their Cardiac Repolarization Parameters for the Procurement of Skin and Blood Samples]; URL: https://www.clinicaltrials.gov; Unique identifier: NCT01338441), and all participants gave written informed consent for participation in the study. We selected 3 cell lines for HS and 3 cell lines for LS groups that showed concordant in vivo and in vitro response to sotalol and with respect to sex (2 women and 1 man in each group).[10] iPSCs were expanded on stem cell–qualified Matrigel-coated (Corning) plates with mTeSR1 (StemCell Technologies). At 80% confluency, cells were passaged using ReLeSR passaging reagent (StemCell Technologies).

Differentiation of iPSCs Into Cardiomyocytes

At 90% confluency, iPSCs were placed in Roswell Park Memorial Institute (RPMI)–1640 medium (Life Technologies) supplemented with B27 without insulin (Life Technologies) and 6 µM CHIR-99021 (Abcam). After 48 hours, the medium was changed to RPMI-1640-B27 without insulin. The following day, the medium was replaced with RPMI-1640-B27 without insulin supplemented with 5 µM IWR-1 (Sigma). By day 5, cells were cultured in RPMI-1640-B27 without insulin and then switched into RPMI1640-B27 with insulin after 48 hours. On day 11, beating iPS-CMs were subjected to glucose starvation in RPMI-1640-B27 without glucose (Life Technologies) for 3 days. Cells were then dissociated using 0.05% trypsin (Life Technologies) for 5 minutes and seeded at a 1.2×10^6 cells/well density. The following day, the medium was switched to RPMI-B27 with insulin for 24 hours, after which the cells were subjected to a second round of glucose starvation for 3 days. By day 18, cells were cultured in RPMI1640-B27 with insulin and the medium was changed every 2 days. All experiments were performed around day 30 of differentiation.

Immunofluorescence

iPSCs and iPS-CMs at day 30 of differentiation were plated on Matrigel-coated coverslips. Cells were then fixed in 4% paraformaldehyde for 15 minutes, permeabilized with Triton X-100, blocked with 2% bovine serum albumin (BSA), and incubated overnight with appropriate primary antibodies (Table S1). The cells were then probed with appropriate conjugated secondary antibodies and stained with DAPI. Immunostaining was examined using a Leica SPE confocal system.

For CAVIN1 (caveolae associated protein 1)/CAV1 (caveolin-1) immunostaining, cells were permeabilized and blocked with 0.05% saponin in 0.2% BSA in phosphate-buffered saline for 20 minutes. Coverslips were incubated on 30-µL droplets of primary antibodies (Table S1) in saponin/BSA for 45 minutes. After 3 washes in saponin/BSA, coverslips were incubated on 30-µL droplets of secondary antibodies in saponin/BSA for 30 minutes. Coverslips were mounted in Fluoromount-G with DAPI (Thermo Fisher). Pictures were acquired with a Nikon A1R confocal microscope equipped with a CFI Plan Lambda S 40× NA 1.25 silicone immersion objective with a resonant scanner. Pictures were processed with Denoise.ai and 3D deconvolution plugins in NIS Elements software (Nikon). Analysis was performed on ImageJ software (National Institutes of Health).

Electrophysiological Assessment

Field Potential Recording

Field potential (FP) recording was conducted using 6-well multielectrode array (MEA) arrays (60-6 well MEA 200/30 iR-Ti-rcr; Multichannel Systems) or 1-well MEA arrays (MEA 200/30 iR-Ti-rcr; Multichannel Systems). Four days before recording, iPS-CMs were dissociated using Enzyme T (Miltenyi Biotec) for 10 minutes at 37 °C, and seeded on the electrode array coated with Matrigel at a density of 200 000 cells/3 µL medium. After 4 hours, RPMI-1640-B27 insulin medium was added to the system. The medium was changed every other day. Each drug (sotalol [Selleckchem], E4031 [StressMarq], clarithromycin [Selleckchem], and vandetanib [Selleckchem]) was prepared at different concentrations in RPMI medium supplemented with B27 and insulin and directly added to wells during recording at 37 °C. Methyl-β-cyclodextrin (MβCD; Sigma) and Dynasore (Sigma) were added respectively 15 minutes and 60 minutes before the recordings and pharmacological stimulations. FP was recorded using Cardio 2D software (Multichannel Systems) for 3 minutes for each condition preceded by 3 minutes of stabilization after drug treatment. Raw MEA data were analyzed using Cardio 2D+ (Multichannel Systems). FP values were averaged from 2 minute recordings by the software. Field potential duration (FPD) was then determined and normalized to peak-to-peak duration using the Frederica formula, as follows: $FPDc = FPD/\sqrt[3]{(\text{peak-to-peak duration})}$.

Patch Clamp

On days 21 to 24 of differentiation, iPS-CMs were dispersed as single cells using Enzyme T (Miltenyi Biotec) for 10 minutes at 37 °C and plated at 60 000 cells/35-mm Petri dish. After 10 to 14 days from seeding, patch-clamp recordings were performed using an Axopatch 200B amplifier controlled by Axon pClamp 11 software through an A/D converter (Digidata 1440B). All recordings were conducted at 37 °C. In current clamp, stimulation was performed using custom-made software running on RT-Linux and an A/D converter (National Instrument PCI-6221) connected to the current command of the amplifier.[12] Data were collected from at least 3 independent differentiations from each group and analyzed using Clampfit 11 software (Molecular Devices).

Current Clamp

Action potential (AP) was acquired in a perforated-patch configuration using 0.22 mM amphotericin-B (Sigma). Cells were constantly perfused using Tyrode solution containing 140 mM sodium chloride (NaCl), 4 mM potassium chloride (KCl), 1 mM calcium chloride ($CaCl_2$), 0.5 mM magnesium chloride ($MgCl_2$), 10 glucose, and 10 mM HEPES (pH 7.4 adjusted with sodium hydroxide [NaOH]). Patch pipettes (tip resistance 3–5 MΩ) were filled with a solution containing 125 mM K-gluconate, 20 mM KCl, 5 mM NaCl, 5 mM HEPES (pH 7.2

adjusted with potassium hydroxide [KOH]), and amphotericin B. After 2 minutes of spontaneous AP recording, cells were paced with 1 ms 30 to 50 pA/pF stimulation pulse at 500 and 700 ms of cycle length. AP classification into ventricular type was determined from the evaluation of the ratio (AP duration [APD30]—APD40)/(APD70—APD80)>1.45, which reflects the presence of a plateau phase. Seven consecutive APs were superposed and averaged. Sotalol solubilized in dimethyl sulfoxide (DMSO) was used at 30-, 50-, and 100-µM concentrations in a solution containing 140 mM NaCl, 4 mM KCl, 1 mM $CaCl_2$, 0.5 mM $MgCl_2$, 30 mM mannitol, and 10 mM HEPES (pH 7.4 adjusted with NaOH).

I_{Kr} Recordings in iPS-CMs

I_{Kr} recordings were performed in the ruptured whole-cell configuration. Voltage clamp protocols are depicted in the corresponding figures. Borosilicate pipettes with 3 to 4 MΩ tip resistance were used for recordings at 1 KHz low-pass filter and filled with a solution containing 140 mM KCl, 5 mM EGTA, 4 mM MgATP, 1 mM HEPES, and 1 mM $MgCl_2$. Current densities were calculated by dividing the current value by membrane capacitance (Cm). A steady-state activation curve was fitted using Boltzmann equation.

Reverse Transcription Quantitative Polymerase Chain Reaction

Total RNA was isolated using NucleoSpin RNA kit (Macherey-Nagel) and reverse transcribed using SuperScript IV VILO Master Mix (Thermo Fisher Scientific). Quantitative polymerase chain reaction was carried out with SYBR Select Master Mix (Applied Biosystems) using the primers listed in Table S2. Gene expression was determined according to the $\Delta\Delta$Ct method after normalization to the expression of the housekeeping *RPL32* gene.

Protein Extraction

Total Protein Lysate

Total protein was extracted using a lysis buffer containing 1% TritonX-100; 100 mM NaCl, 50 mM Tris-HCl, 1 mM EGTA, and 1 mM sodium orthovanadate (Na_3VO_4); 50 sodium fluoride (NaF); phosphatase inhibitor cocktails 2 and 3 (P0044 and P5726; Sigma-Aldrich); and a protease inhibitors cocktail (P8340; Sigma-Aldrich). Extracted samples were sonicated and centrifuged at 15 000×*g* for 15 minutes at 4 °C. Protein quantification was performed using Pierce BCA Protein Assay Kit (Thermo Fisher).

Cell Fraction Isolation

Proteins from the cytoplasm, membrane, nucleus, and cytoskeleton compartments were isolated from at least 5 million cells per condition using Qproteome Cell Compartment Kit (Qiagen), as per manufacturer instructions. Extracted proteins were precipitated using acetone, solubilized in the lysis buffer mentioned previously, and quantified using Pierce BCA Protein Assay Kit (Thermo Fisher). Fractioning was validated by revealing a specific protein from each cell compartment.

Viral Infection

On days 21 to 23 of differentiation, cardiomyocytes were infected with an adenovirus carrying cytomegalovirus promoter driving CAVIN1 (plus a T2A separating EGFP [VB190717-1058jag]) and adenovirus carrying cytomegalovirus driving GFP (VB150925-10024) only as a control (Vector Builder) at a multiplicity of infection of 50 overnight. The medium was replaced with fresh RPMI-1640-B27 with insulin supplemented with 5% fetal bovine serum. Seven days after the infection, iPS-CMs were used for experiments.

CAVIN1 Silencing

Small interfering RNA (siRNA) targeting *CAVIN1* (siCAVIN1; s49507), nontargeting siRNA (siNeg; 4390843), and GAPDH silencer (siGAPDH; 4390849) were purchased from Thermo Fisher Scientific. GAPDH siRNA was used to determine the optimal siRNA quantity that allowed maximum knockdown, and 200 nM siRNA was sufficient to induce 70% reduction in the RNA expression of GAPDH and was used for the following transfection. On day 24 to 25 of differentiation, transfection with either siCAVIN1 or siNeg was performed using Lipofectamine RNAiMAX Transfection Reagent (Thermo Fisher Scientific) as per manufacturer instructions. Cells were used after 5 days of transfection.

Statistical Analysis

The number of samples and replicates used in each experiment are recorded in the text and figure legends. Results are expressed as mean±SEM. Two-group comparisons were made using nested *t* tests, and more than 2-group comparisons were performed using mixed effect models. $P<0.05$ was considered statistically significant. Statistical analyses were performed with GraphPad Prism software (version 10).

RESULTS

Patient-Specific iPS-CMs Recapitulate Interindividual Variability in Sotalol Sensitivity

We used 6 lines from our previously developed library of patient-specific iPSCs,[10] 3 of them (2 female and 1 male) derived from individuals with the highest sensitivity (HS) and 3 (2 female and 1 male) with lowest sensitivity (LS) to sotalol (ie, based on the measure of the maximal change in QT interval 3 hours after sotalol administration). Expression of pluripotency markers was validated in all clones (Figure S1A and S1B), and cardiac differentiation efficiency was assessed by immunostaining for cardiac markers (troponin T and α-actinin; Figure S1C) and flow cytometry. Results revealed an average of 98.9% troponin T–positive cells in both groups (Figure S1D). A predominance of the ventricular-like type (≈85%) was observed after analyzing action potential recordings (Figure S1E). The ratio of the ventricular (MYL2) and atrial (MYL7) myosin light chain RNA expression was similar between HS and LS iPS-CMs (Figure S1F).

We then compared the electrophysiological measures of HS and LS iPS-CMs (n=3 different clones for each group) using the patch-clamp technique at the single-cell level and MEA recordings at the tissue level. These iPS-CMs reproduced the clinical phenotype of patients as they exhibited similar electrophysiological measures at baseline and more pronounced prolongation of the repolarization durations in response to sotalol in HS iPS-CMs (Figure 1A through 1F; Figure S2; Table S3). APD90 and APD50 were significantly higher in HS than in LS iPS-CMs at 30- and 50-µM sotalol concentrations (Figure 1D; Figure S2C; Table S3). These results were reproduced at the tissue level (Figures 1G; Table S3). Whereas the late phase of repolarization was affected, 30- and 50-µM sotalol changed neither the early stage of repolarization (APD30; Figure 1C) nor the resting membrane potential (Figure 1B) or the depolarization phase (velocity, amplitude, and overshoot; Figure 1E and 1F; Figure S2D; Table S3). This observation revealed a principal effect of sotalol on late repolarization currents in iPS-CMs derived from patients with high sensitivity to sotalol in vivo.

Sotalol Application Changes hERG Distribution Within HS iPS-CMs

The expression levels of *KCNH2* and other central ion channel genes (*KCNQ1*, *SCN5A*, *CACAN1C*, and *KCNE2*) implicated in congenital LQTS were not different between HS and LS iPS-CMs (Figure 2A; Figure S3A). At the protein level, the mature glycosylated hERG (molecular weight 150 KDa) expressed at the plasma membrane and the nonglycosylated form (molecular weight 135 KDa) were similarly expressed between both groups (Figure 2B). At the functional level, the density and activation properties of I_{Kr}, which is the current generated by hERG channels, were not different between HS and LS iPS-CMs before any pharmacological stimulation (Figure 2C; Figure S3B through S3E). However, I_{Kr} maximum tail current density was significantly and profoundly decreased in HS iPS-CMs after treatment with 50 µM sotalol but remained unchanged in LS iPS-CMs (Figure 2C). Overall, these results indicate a peculiar reactivity of hERG channels in HS iPS-CMs to sotalol. This phenomenon was consistent with a decrease in I_{Kr} that correlates with the higher prolongation of repolarization after sotalol intake, as observed in patients with a predisposition to diLQT.

Total hERG (glycosylated and nonglycosylated) levels were unaffected by sotalol treatment (Figure S4A through S4D). To test whether the decrease in I_{Kr} is associated with altered hERG expression trafficking, we traced hERG distribution in different cellular fractions (Figure S4E) in HS and LS iPS-CMs treated with vehicle (DMSO) or sotalol. hERG expression was significantly lower in the cell membranes but increased in the cytoskeleton-associated fractions of HS iPS-CMs in response to sotalol treatment (Figure 2D and 2E); no significant change in hERG expression was detected in the cytoplasmic fraction (Figure S4F). In contrast, the subcellular expression of hERG was unchanged in all cellular compartments of LS iPS-CMs after sotalol treatment (Figure 2D and 2E). Considering the intact hERG levels in

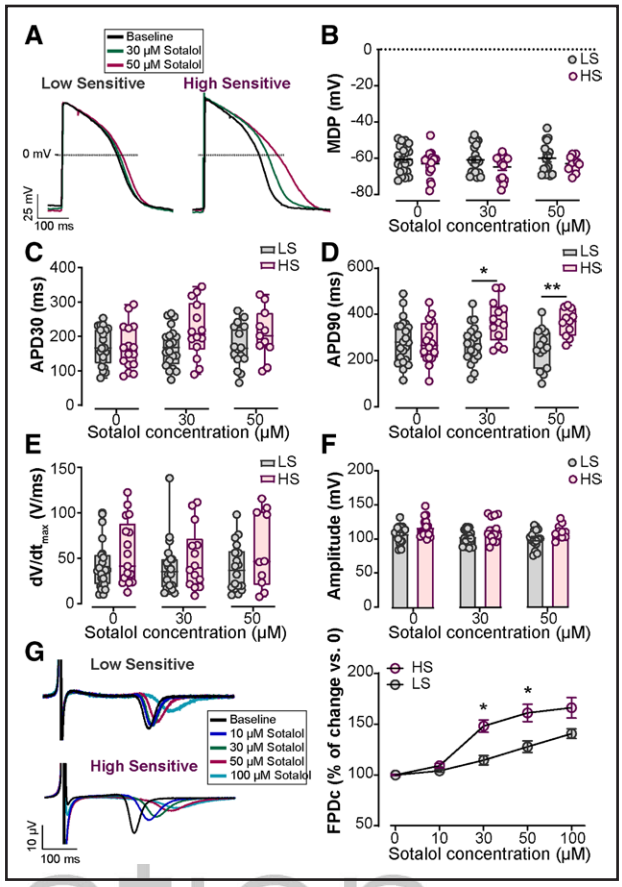

Figure 1. High-sensitivity, but not low-sensitivity, induced pluripotent stem cell–derived cardiomyocytes exhibit a prolongation in the late repolarization phase after sotalol application.

A, Aligned action potentials comparing the baseline with 30- and 50-µM sotalol treatments in the low-sensitivity (LS) and high-sensitivity (HS) induced pluripotent stem cell–derived cardiomyocytes (iPS-CMs). **B**, Membrane diastolic potential (MDP) measured at baseline (0) and after sotalol application (30 and 50 µM) in LS and HS iPS-CMs. **C**, Box whisker blot of action potential duration (APD) at 30% repolarization (early phase) analyzed from LS and HS iPS-CMs paced at 1.5 Hz before and after applying 30 and 50 µM sotalol. **D**, Box whisker blot of APD at 90% repolarization (late phase) analyzed from LS and HS iPS-CMs paced at 1.5 Hz treated or not with 30 and 50 µM sotalol. *P<0.05 and **P<0.01 vs LS iPS-CMs (mixed effect models). **E**, Maximum upstroke velocity dV/dt_{max} calculated in LS and HS iPS-CMs paced at 1.5 Hz after treatment with different concentrations of sotalol. **F**, Upstroke amplitude analyzed from the action potential recorded in HS and LS iPS-CMs treated with different concentrations of sotalol and paced at 1.5 Hz. **G**, **Left**, Aligned field potentials showing the effect of different concentrations of sotalol on LS and HS iPS-CMs. **Right,** Percentage of normalized corrected field potential duration (FPDc) change vs baseline after the application of sotalol. *P<0.05 vs LS iPS-CMs (mixed effect models).

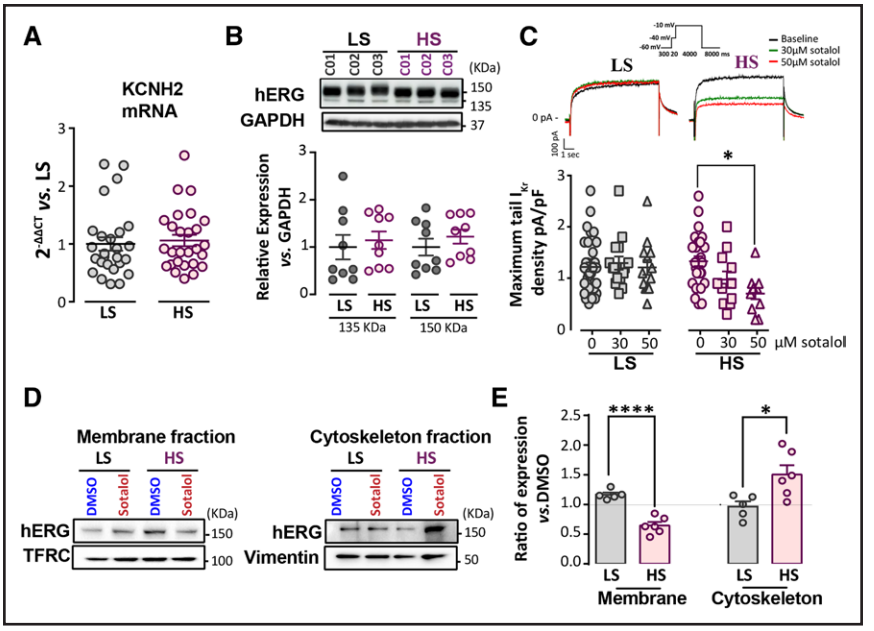

Figure 2. Changes in the repolarization phase of high-sensitivity induced pluripotent stem cell–derived cardiomyocytes after sotalol application are attributable to different hERG distribution within the cell.

A, *KCNH2* mRNA expression level at day 30 of differentiation measured by SYBR green in low-sensitivity (LS) and high-sensitivity (HS) induced pluripotent stem cell–derived cardiomyocytes (iPS-CMs; 10 LS and 10 HS from the complete iPSC library of the iCTEST study [Selections of Subjects With Important Changes in Their Cardiac Repolarization Parameters for the Procurement of Skin and Blood Samples],[10] 2–4 replicates per line). Cts were normalized to RPL32 and the ratio vs LS ($2^{-\Delta\Delta Ct}$) was then calculated. **B**, Representative immunoblot of hERG (human ether-a-go-go-related gene) encoded by *KCNH2* from the total protein lysate at day 30 of differentiation of 3 different clones of LS and HS iPS-CMs and the ratio of membranous hERG of 150 KDa and cytosolic immature hERG of 135 KDa expression normalized to GAPDH (n=3 lines per group with 3 replicates per line, mixed effects model). **C**, **Top**, Superimposed traces for delayed-rectifier potassium current (I_{Kr}) before (black) and after (colored) the application of 30 and 50 µM sotalol in LS and HS iPS-CMs (from 1 cell line in each group); bottom: maximum tail I_{Kr} density without or with application of different concentrations of sotalol. *P<0.05 vs before sotalol application (tested within each group respectively, mixed effect models). **D**, Representative immunoblot of hERG expression in different LS and HS iPS-CM fractions treated with either 0.1% DMSO or 50 µM sotalol for 10 minutes. TFRC (transferrin receptor) and vimentin were used to normalize the plasma membrane and cytoskeleton-associated fraction, respectively. **E**, Ratio of hERG (150 KDa) expression after treatment with 50 µM sotalol vs DMSO in LS and HS iPS-CMs. *P<0.05 and ****P<0.0001 vs LS iPS-CMs, respectively (n=3 lines per group with 1–2 replicates per line, mixed effects model).

the cytoplasmic fraction, we decided to exclude this fraction from further investigations. Overall, our results are in line with the original mechanism where higher susceptibility to develop abnormal cardiac repolarization in response to an offending drug is supported by the drug-induced translocation of targeted channels from the membrane to the cytoskeleton-associated fractions.

CAVIN1 Expression Level Determines Sensitivity to Sotalol

Among the 5 differentially expressed genes (*CAMKV*, *DLG2*, *KCNE4*, *HTR2C*, and *CAVIN1*) previously identified,[10] we confirmed the higher mRNA expression of *CAVIN1* in HS than in LS iPS-CMs (Figure 3A); however, no significant differences in the expression of other candidates were found (Figure S5). The protein expression of CAVIN1 (also called PTRF) was also 2-fold higher in HS iPS-CMs than in LS iPS-CMs (Figure 3B). In line with our electrophysiological observations, CAVIN1 appeared as an appealing candidate previously reported to be required for the biogenesis of caveolae, a type of cell membrane structure containing cardiac ion channels.[13] Immunostaining analyses confirmed the expression of CAVIN1 in α-actinin–positive iPS-CMs (Figure 3C). The expression of CAVIN1 at the plasma membrane was found to colocalize with that of CAV1 (Figure 3C), indicating the presence of bona fide caveolae in our iPS-CMS.

To further investigate the role of CAVIN1 in the repolarization response to sotalol, we performed experiments that reversed CAVIN1 expression in HS and LS groups. First, we overexpressed CAVIN1 in LS iPS-CMs using an adenovirus harboring *CAVIN1*. Seven days after infection, the protein expression of CAVIN1 increased by ≈10-fold compared with that in LS iPS-CMs infected with the control GFP adenovirus (Figure S6A). MEA recordings showed a significant change in the response of LS iPS-CMs overexpressing CAVIN1 to sotalol. Sotalol application induced a significant prolongation in the repolarization duration compared with controls (Figure 3D), thus mimicking the effect observed in HS iPS-CMs (Figure 1G). The beating rate changed at 100-µM sotalol concentrations (Figure S6B). Then,

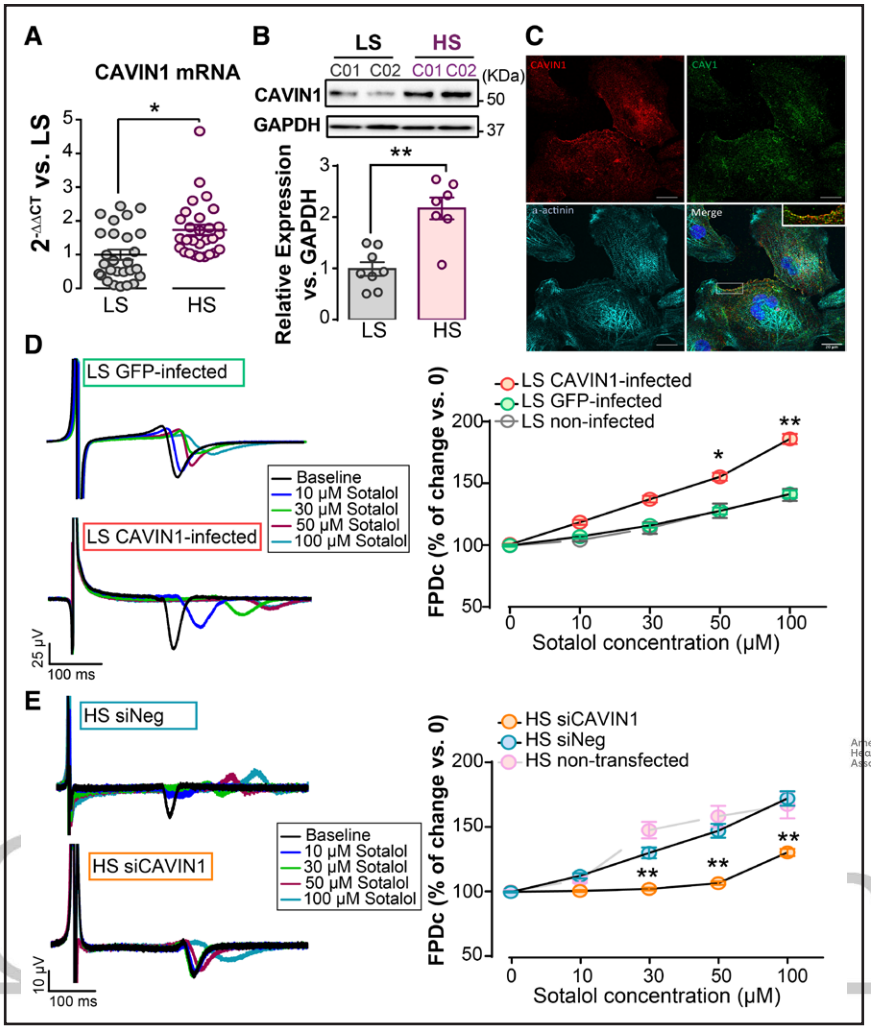

Figure 3. Modulation of CAVIN1 expression in high-sensitivity and low-sensitivity induced pluripotent stem cell–derived cardiomyocytes is sufficient to reverse the changes in the repolarization duration in response to sotalol.
A, Comparison of *CAVIN1* mRNA expression level between low-sensitivity (LS) and high-sensitivity (HS) induced pluripotent stem cell–derived cardiomyocytes (iPS-CMs). Cts were normalized to RPL32 and the ratio vs LS ($2^{-\Delta\Delta Ct}$) was then calculated. *P<0.05 vs LS iPS-CMs (nested t test). **B**, **Top,** Representative immunoblot illustrating CAVIN1 (caveolae associated protein 1) expression in LS and HS iPS-CMs originating from 2 different lines; bottom: expression level of CAVIN1 in total protein lysate extracted from LS and HS iPS-CMs normalized to GAPDH (n=3 lines per group with 2–3 replicates per line). **P<0.01 vs LS iPS-CMs (nested t test). **C**, Representative confocal images for immunostainings of CAVIN1 (red), CAV1 (caveolin-1; green), and the cardiac marker α-actinin (cyan) in HS iPS-CMs. Nuclei are stained in blue using DAPI. Insert in the merge image shows the colocalization of CAVIN1 and CAV1 at the plasma membrane in iPS-CMs. **D**, **Left,** Representative aligned field potential recorded from LS iPS-CMs infected with either GFP or CAVIN1 adenovirus before and after applying different concentrations of sotalol. **Right,** Percentage of change compared with baseline of corrected field potential duration (FPDc) measured in LS iPS-CMs infected with either GFP (green) or CAVIN1-T2A-GFP adenovirus (red) in response to increasing concentrations of sotalol. FPDc values from noninfected LS iPS-CMs are presented in gray. *P<0.05 and **P<0.01 vs GFP-infected LS iPS-CMs, respectively (mixed effect models). **E**, **Left,** Superimposed field potential recorded from HS iPS-CMs 5 days after the transfection with either siNeg or siCAVIN1 before and after application of increasing concentrations of sotalol; right: percentage of change compared with baseline FPDc measured in HS iPS-CMs transfected with siNeg or siCAVIN1. FPDc values from nontransfected HS iPS-CMs are plotted in pink. **P<0.01 vs siNeg-transfected HS iPS-CMs, respectively (mixed effect models).

we knocked down *CAVIN1* expression in HS iPS-CMs after verifying 200 nM of siRNA as the optimal quantity to induce maximal RNA reduction (Figure S6C). Five days after *CAVIN1*-siRNA transfection, CAVIN1 expression decreased by 84% at the RNA level (Figure S6D) and 62% at the protein level (Figure S6E). This reduction in the CAVIN1 expression in HS iPS-CMs changed their reaction to sotalol, as evident from a significantly lower reactivity to 30-, 50-, and 100-μM concentrations of sotalol (Figure 3E) without any change in the beating rate as compared with siNeg-transfected cells (Figure S6F). Hence, CAVIN1 expression modulation was sufficient to strongly reverse the specific phenotypes observed in our patient-specific iPSC library, indicating CAVIN1 as a significant driver of individual susceptibility to the drug response.

Depletion of Caveolae Limits the Effect of CAVIN1 on Sotalol Sensitivity

To further address the involvement of caveolae, we first visualized the presence of caveolae at the plasma membrane of iPS-CMs using transmission electron microscopy (Figure S7A and S7B). In line with the central role of CAVIN1 in caveolae biogenesis,[14] we observed that the caveolae density at the plasma membrane of HS iPS-CMs was significantly decreased after treatment with CAVIN1 siRNA compared with control (Figure 4A). In concordance, the expression of CAV3 (caveolin-3) was increased in LS iPS-CMs overexpressing CAVIN1 (Figure S7C). The presence of CAV1, another essential element in caveolae biogenesis besides CAVIN1, was detected in the cytoskeleton-associated fraction of iPS-CMs (Figure 4B), consistent with the role of the cytoskeleton in caveolae distribution at the plasma membrane.[15] CAV1 expression increased in LS iPS-CMs infected with CAVIN1 compared with that in controls (Figure 4B), thereby confirming the relationship between CAVIN1 expression and caveolae formation in iPS-CMs. Contrary to CAVIN1, *CAV1* and *CAV3* transcript levels were similar between LS and HS iPS CMs at baseline (Figure S7D).

To evaluate the presence of hERG channels in caveolae, we then treated cells with MβCD, a detergent that removes cholesterol from the membrane and, thus, removes caveolae. The application of 1 mM MβCD significantly prolonged the repolarization phase before any pharmaceutical stimulation, indicative of the elimination of a repolarizing channel from caveolae by MβCD (Figure 4C). To assess whether this channel is hERG, we isolated proteins from different cellular compartments after treatment with either 5 mM MβCD or vehicle (water). Immunoblots revealed the decrease in hERG expression in the membranous fraction and its accumulation in the cytoskeleton-associated fractions after MβCD (Figure 4D). Thus, the localization of hERG depends on the distribution of cholesterol-enriched fractions. The sensitivity to sotalol was also significantly affected by the removal of caveolae by MβCD. Treatment of HS iPS-CMs with 1 mM MβCD for 15 minutes strongly reduced the prolongation of repolarization duration upon sotalol application (Figure 4E). MβCD-mediated caveolae disruption in LS iPS-CMs overexpressing CAVIN1 significantly limited the prolongation in FPDc at different sotalol concentrations (Figure S8). We further assessed the dependence of the process on active endocytosis by using Dynasore, a molecule that blocks dynamin, the protein responsible for caveolar scission from the plasma membrane.[16] Treating the HS iPS-CM with 50 μM Dynasore for 1 hour before electrophysiological recordings led to a nonsignificant reduction of the exacerbated response of the HS iPS-CMs to sotalol, to a level similar to the one observed with LS iPS-CMs (Figure 4F). Overall, these data suggest a link among CAVIN1, caveolae biogenesis and location, and increased sensitivity to sotalol.

CAVIN1 Enhances hERG Channels Turnover in HS iPS-CMs After Sotalol Treatment

We further investigated the expression of different forms of hERG channel (the predominant isoform in adult heart hERG1a 150 KDa, hERG1b 120 KDa, and degraded hERG 70 KDa) in response to sotalol. We first observed that the decrease in the mature hERG1a channel expression in the membrane compartment after sotalol treatment (Figure 2D) was associated with a significant increase in the fragmented form of hERG (Figure 5A) in the cytoskeleton-associated fraction of HS iPS-CMs compared with that in LS iPS-CMs (Figure 5A). To assess the possibility of hERG trafficking back to the membrane, we compared the recruitment of RAB11, a marker of recycling endosomes, which was mainly detected in the membrane fraction and was more expressed in HS iPS-CMs treated with sotalol than those treated with DMSO. However, in LS iPS-CMs, RAB11 expression level was similar after treatment with sotalol or DMSO (Figure 5B). Overall, sotalol treatment of HS iPS-CMs induced hERG association with vesicles where some were fragmented, and others were recycled back to the surface.

We finally tested whether this mechanism is CAVIN-1 dependent. We analyzed hERG expression in the different fractions in response to sotalol in HS iPS-CMs treated with siRNA against CAVIN1 or control. The process involving the reduction of the mature hERG1a channel (150 KDa) in cellular membranes and the accumulation of the fragmented form of hERG in the cytoskeleton-associated fraction of HS iPS-CMs after sotalol treatment was not observed anymore after CAVIN1 silencing compared with control (Figure 5C and 5D; Figure S9). These results further confirm that CAVIN1 contributes to the increased ratio of cytoskeleton fraction versus membrane fraction of hERG channels in response to sotalol treatment.

CAVIN1-Dependent hERG Channels Respond to Other hERG Blockers

We measured the response of our patient-specific iPS-CMs to other drugs targeting hERG, including E4031, a known blocker of hERG channel; vandetanib, an anticancer drug with medium risk of torsade de pointes; and clarithromycin, an antibiotic with a low risk of torsade de pointes. In comparison with LS iPS-CMs, HS iPS-CMs developed significant prolongation in FPDc after treatment with 0.1 and 1 μM of E4031, and a nonsignificant trend for prolongation with vandetanib and clarithromycin (Figure 6A through 6C). These results suggest that the particular susceptibility to develop abnormal

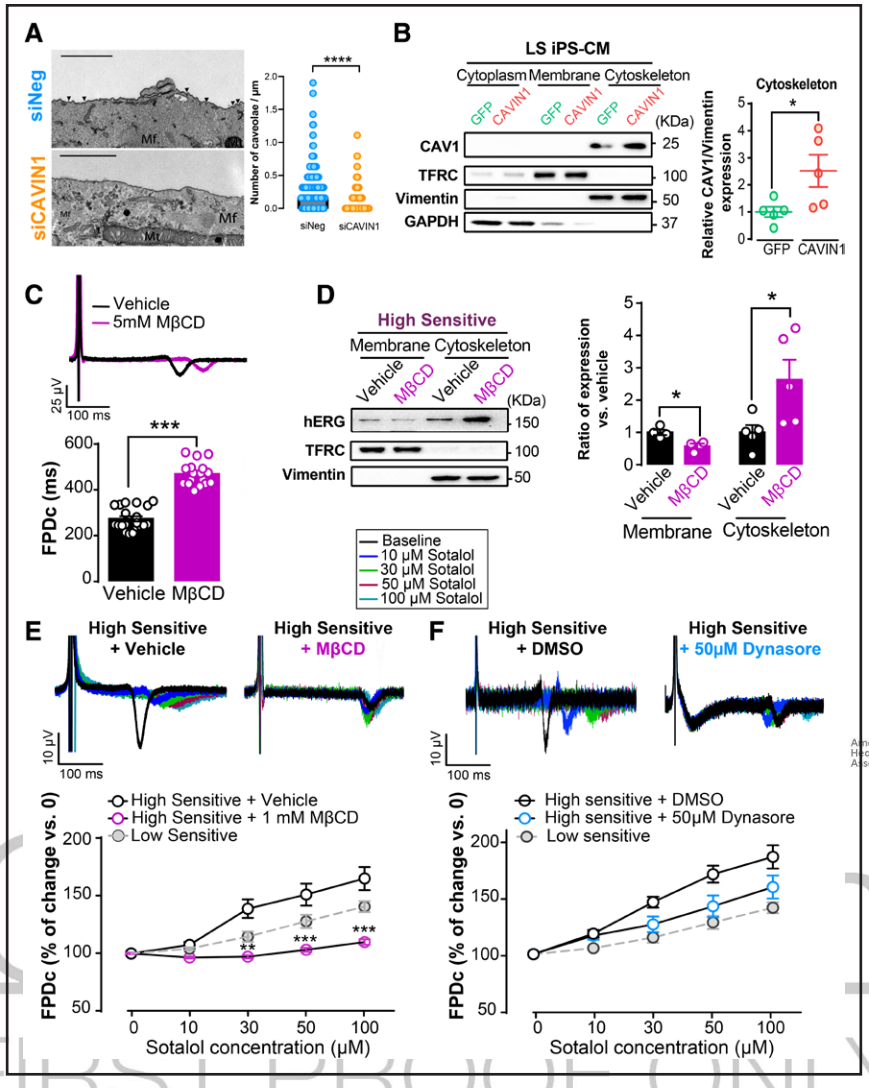

Figure 4. Depletion of caveolae limits CAVIN1 effect on the repolarization phase.
A, **Left,** Transmission electron microscopy images showing caveolae at the plasma membrane (omega-shaped invaginations indicated with arrowheads) in high-sensitivity (HS) induced pluripotent stem cell–derived cardiomyocytes (iPS-CMs) treated with scrambled (siNeg) and small interfering RNA (siRNA) against CAVIN1 (caveolae associated protein 1; siCAVIN1). Right: quantification of the caveolae density on the cell plasma membrane in siNeg (335 images) and siCAVIN1 (335 images) treated iPS-CMs. ****P<0.0001 nested t test; scale=1 µm. **B**, **Left**, Immunoblots displaying CAV1 protein expression in different cell compartments and the housekeeping genes for each fraction (TFRC [transferrin receptor], vimentin, and GAPDH for the membrane, cytoskeleton, and cytoplasmic fraction, respectively) in iPS-CMs infected with either GFP or CAVIN1 adenovirus. **Right**, Ratio of CAV1 expression in the cytoskeleton fraction of low-sensitivity (LS) iPS-CMs at day 7 of infection with GFP and CAVIN1-Adv. *P<0.05 vs LS iPS-CMs (nested t test). **C**, **Top,** Representative recordings of field potential of HS iPS-CMs treated with either 1 mM of methyl-β-cyclodextrin (MβCD) for 15 minutes at 37 °C or vehicle (water). **Bottom,** Corrected field potential duration (FPDc) is compared. ***P<0.001 vs vehicle (nested t test). **D**, **Left,** Representative immunoblot of membranous and cytoskeletal hERG (human ether-a-go-go-related gene) isolated from HS iPS-CMs treated with 5 mM MβCD for 15 minutes at 37 °C or vehicle. TFRC and vimentin were used as loading references for the plasma membrane and cytoskeleton, respectively. Right: hERG expression was normalized to each loading reference (n=2 HS lines, 2–3 replicates). *P<0.05 vs HS iPS-CMs treated with vehicle (nested t test). **E**, **Top,** Representative superimposed field potentials recorded from HS iPS-CMs treated with either 1 mM MβCD or vehicle for 15 minutes at 37 °C. The 3 HS iPS-CMs lines were then treated with increasing concentrations of sotalol (with at least 2 independent differentiations per conditions). **Bottom**, Percentage of change compared with baseline was calculated and plotted. **P<0.01 and ***P<0.0001 vs HS iPS-CMs treated with vehicle (mixed effect models). **F**, **Top,** Aligned field potentials recorded from HS iPS-CMs treated with either 0.1% DMSO or 50 µM Dynasore for 1 hour at 37 °C. Different concentrations of sotalol were then applied. **Bottom,** Percentage of change compared with baseline was calculated and plotted. Mf indicates myofibril; and Mt, mitochondria.

repolarization in response to sotalol extends to other hERG blockers. Cardiomyocytes from patients presenting high sensitivity to sotalol exhibit similar sensitivity to other hERG blockers. One may speculate whether the abnormal response to these hERG blockers is also mediated by CAVIN1. In line with the observations reported with sotalol, CAVIN1 overexpression in LS iPS-CMs or silencing in HS iPS-CMs mediated significant changes

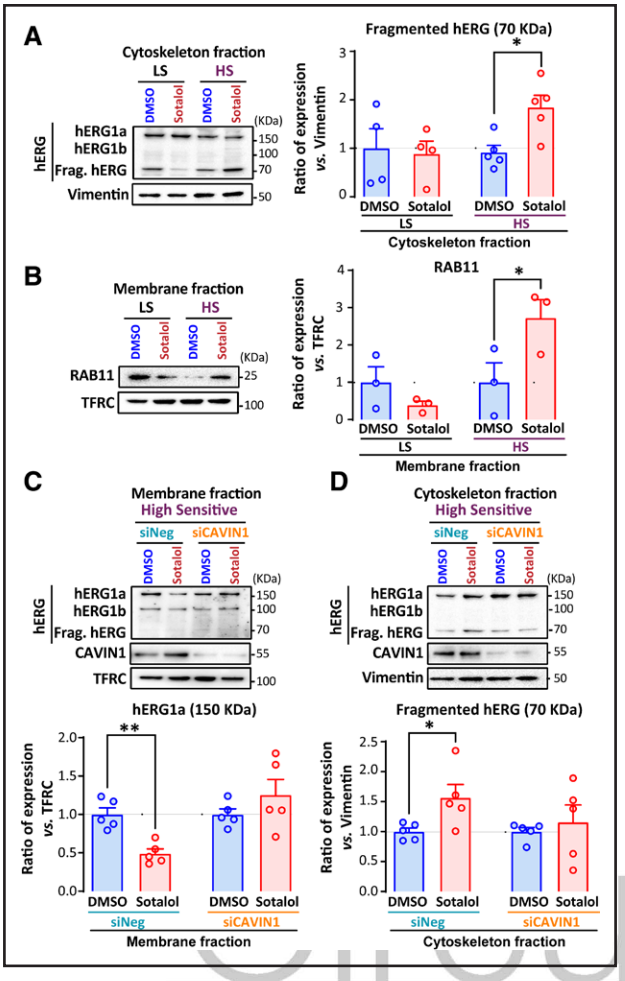

Figure 5. CAVIN1 increases hERG translocation upon sotalol treatment in high-sensitivity induced pluripotent stem cell–derived cardiomyocytes.

A, **Left,** Representative immunoblot of hERG (human ether-a-go-go-related gene) at different molecular weights (hERG1a, hERG1b, and fragmented hERG at 150, 110, and 70 KDa, respectively) in low-sensitivity (LS) and high-sensitivity (HS) induced pluripotent stem cell–derived cardiomyocyte (iPS-CM) cytoskeletal fraction treated with either 0.1% DMSO or 50 µM of sotalol for 10 minutes. Vimentin was used as a loading reference for the cytoskeleton fraction. **Right,** Ratio of fragmented hERG (70 KDa) after treatment with sotalol vs DMSO in LS and HS iPS-CMs (n=3 cell lines per group with 1 to 2 replicates per cell line). *P<0.05 vs LS iPS-CM, respectively (mixed effects model). **B**, **Left,** Representative immunoblot of RAB11 and TFRC (transferrin receptor) in the membranous fraction of LS and HS iPS-CMs treated with sotalol or DMSO. RAB11 bands were normalized to TFRC. **Right**, *P<0.05 vs treatment with DMSO (n=3 lines per group, mixed effects model) **C**, **Top**, Representative immunoblot showing hERG and CAVIN1 (caveolae associated protein 1) as well as the loading reference of the membrane fraction (TFRC) in HS iPS-CMs transfected with either siNeg or siCAVIN1 and then exposed to DMSO or sotalol. **Bottom,** Quantification of mature hERG1a (150 KDa) expression at the plasma membrane normalized to TFRC and ratio compared with DMSO in HS iPS-CMs transfected with CAVIN1 small interfering RNA (siRNA) or negative siRNA. **P<0.01 vs treatment with DMSO (n=3 lines per group with 1 to 2 replicates per line, mixed effects model). **D**, **Top**, Representative immunoblot of hERG, CAVIN1, and vimentin in the cytoskeleton of HS iPS-CMs transfected with either siNeg or siCAVIN1 and then treated with DMSO or sotalol. Bottom: fragmented form of (*Continued*)

Figure 5 Continued. hERG (70 KDa) in the cytoskeleton normalized to vimentin and ratio compared with DMSO in HS iPS-CMs transfected with negative siRNA. *P<0.05 vs treatment with DMSO (n=3 lines per group with 1 to 2 replicates per line, mixed effects model).

in the response to these hERG blockers. CAVIN1 overexpression induced a more significant change in the cardiac repolarization duration of LS iPS-CMs after treatment with E4031, and a nonsignificant trend for prolongation with vandetanib and clarithromycin (Figure 6D through 6F). CAVIN1 silencing abrogated the reactivity to increasing concentrations of hERG blockers in HS iPS-CMs (Figure 6G through 6I). Taken together, cardiomyocytes presenting high sensitivity to sotalol are also sensitive to other hERG blockers, and CAVIN1 expression level drives the cellular responses to these blockers.

DISCUSSION

This study uncovers a new role of CAVIN1 in mediating susceptibility to diLQT syndrome. Higher expression of CAVIN1 promoted higher turnover of hERG channels from the membrane to the cytoskeleton-associated fractions in response to hERG blockers, leading to an excessive prolongation of the repolarization phase. CAVIN1 expression was significantly higher in iPS-CMs from patients predisposed to diLQT in vivo, and CAVIN1 expression modulation was sufficient to shift the cell's response to hERG blockers. A progressive prolongation of the repolarization phase was observed in LS iPS-CMs with increasing sotalol concentrations, likely reflecting the direct pharmacological inhibition of hERG. In contrast, the higher response to low concentrations of sotalol observed in HS iPS-CMs resulted from an additional mechanism associated with an unbridled internalization of hERG by a CAVIN1/caveolae-dependent process.

CAVIN1 exerts a pivotal role in the biogenesis of caveolae, which are membrane invaginations enriched in cholesterol[17] and associated with hERG channels.[18,19] Variants in *CAVIN1* cause lipodystrophy and have been previously associated with congenital LQTS, but the precise mechanism is questionable.[20] CAVIN1 expression level is positively correlated with the number of caveolae at the cardiomyocytes' membrane,[21] consistent with our results showing elevated expression of CAV1 and CAV3, the signature proteins of caveolae, in CAVIN1-infected cells, and reduction in caveolae density at the membrane after CAVIN1 knockdown. *CAV3* variants have been associated with congenital long QT syndrome type 9, and CAV3 can affect the availability of hERG channels at the cell membrane.[22] Previous studies have reported that the clathrin-independent pathway, including caveolae, mediates hERG endocytosis under physiological conditions.[14,19,23–25] Our results demonstrate the involvement

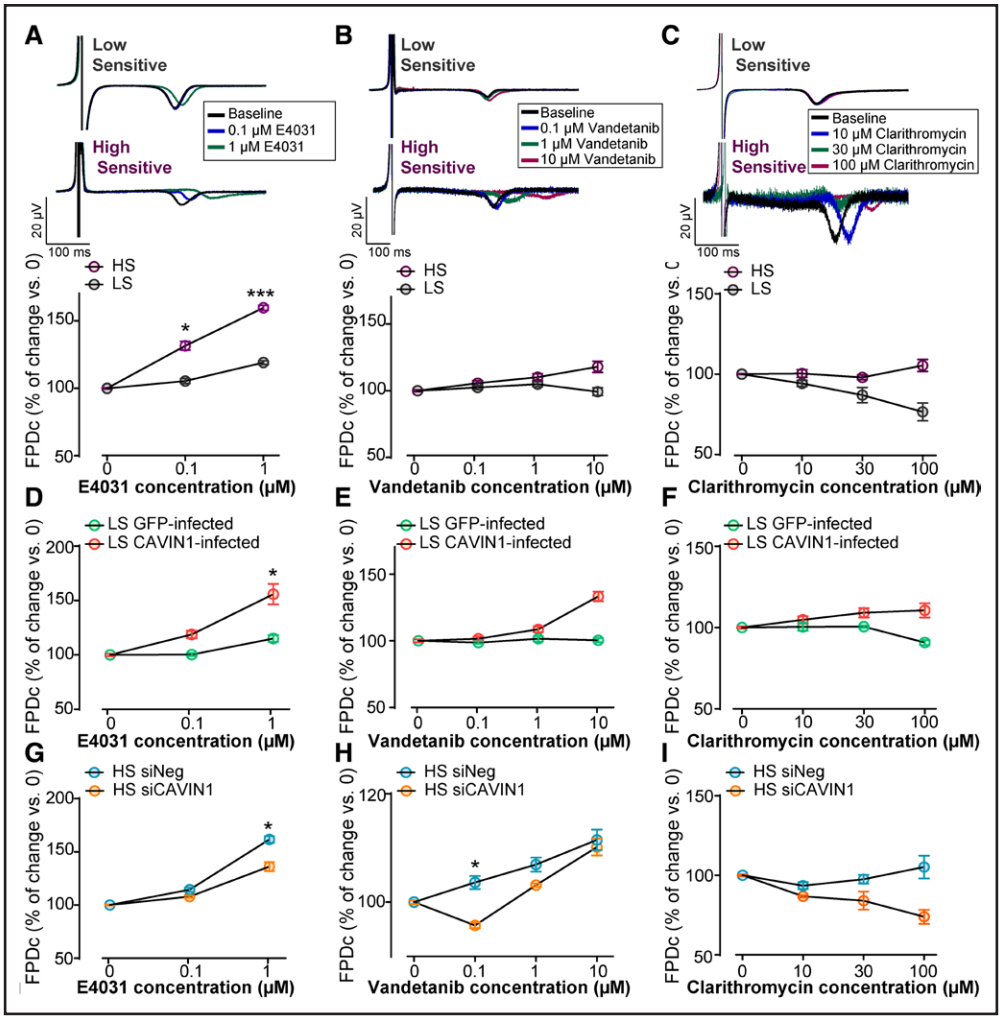

Figure 6. Universal mechanism implicating CAVIN1 in response to other hERG blockers.
A, **Top**, Representative superimposed noncorrected field potential (FP) recorded from low-sensitivity (LS) and high-sensitivity (HS) induced pluripotent stem cell–derived cardiomyocytes (iPS-CMs) after treatment with different concentrations of E4031. Bottom: averaged percentage of change in corrected field potential duration (FPDc; corrected to beating frequency) compared with that at baseline after application of 0.1 and 1 µM E4031. *P<0.05 and ***P<0.001 vs LS iPS-CMs (mixed effect models). **B**, **Top,** Aligned noncorrected FP recorded from LS and HS iPS-CMs treated with different concentrations of vandetanib. Bottom: averaged percentage of change in FPDc (corrected to beating frequency) compared with that at baseline after application of 0.1, 1, and 10 µM of vandetanib (mixed effect models). **C**, **Top**, Aligned noncorrected FP recorded from LS and HS iPS-CMs treated with different concentrations of the antibiotic clarithromycin. **Bottom**, Averaged percentage of change in FPDc (corrected to beating frequency) compared with that at baseline after application of 10, 30, and 100 µM of clarithromycin. **D** through **F**, Averaged percentage of change in FPDc compared with that at baseline measured in LS iPS-CMs infected with either GFP or CAVIN1-T2A GFP adenoviruses in response to increasing concentrations of E4031, vandetanib, and clarithromycin. *P<0.05 vs GFP-infected LS iPS-CMs, respectively (mixed effect models). **G** through **I**, Percentage change in FPDc compared with that at baseline after application of different concentrations of (from left to right) E4031, vandetanib, and clarithromycin at day 5 of transfection of HS iPS-CMs with either siNeg or CAVIN1 small interfering RNA. *P<0.05 vs GFP-infected LS iPS-CMs, respectively (mixed effect models).

of caveolae and CAVIN1 in the subcellular location of hERG channels. hERG translocation from the plasma membrane to the cytoskeleton is rapidly activated in the presence of hERG blocker and is pathologically excessive in HS individuals who are thus predisposed to develop diLQT.

The distribution of caveolae at the plasma membrane is controlled by the elements of the cytoskeleton, notably microtubules and actin filaments.[15] We observed expression of caveolae markers in the cytoskeleton protein fraction of iPS-CMs, suggesting that the plasma membrane and the cytoskeleton are 2 key compartments for hERG channels. Depletion of caveolae was able to decrease the excessive repolarization response to sotalol. Our results suggest that CAVIN1 is required for the proper location of hERG channels between the membranes and the cytoskeleton-associated fractions after sotalol application. Once internalized, membrane proteins undergo different steps, including trafficking to degradation or recycling back to the membrane surface.[26] We observed an accumulation of the cleaved form of hERG (70 kDa)[27–29] in HS iPS-CMs after sotalol

exposure, suggesting that hERG channels are, at least in part, degraded after CAVIN1-dependent translocation. *CAVIN1* silencing was associated with a reduction in fragmented hERG level. The synthesis process of hERG channels is slow, and hERG recycling back to the membrane is essential to maintain its stable surface expression and ensure fast recovery of the repolarization duration.[30] Trafficking toward the membrane is notably mediated by the GTPase RAB11.[30–33] Our protein fractioning data showed higher recruitment of RAB11 to the membrane in HS iPS-CMs than in LS iPS-CMs after treatment with sotalol. These results are indicative of an increase in recycling endosomes and acceleration of the protein turnover to rescue hERG density at the surface membrane, and may explain why QT interval returns to normal after discontinuation of the drug.

Previous studies have attempted to improve our understanding of the genetic predisposition to diLQT.[6,8,9] Despite some association with genetic variants, especially on the *KCNH2* gene, the large majority of diLQT cases remain genetically unresolved.[8] In contrast to these studies, we herein identified higher expression of CAVIN1 as a key molecular mechanism to explain the repolarization delay in response to hERG blockers. Hence, future studies should be devoted to understanding the regulation of CAVIN1 expression and why CAVIN1 expression is physiologically higher in some individuals. There are no known genetic variants of *CAVIN1* associated with the regulation of its expression. Moreover, it is well established that women are at a higher risk of diLQT than men and that contraceptive pills can aggravate this risk.[34] Female sex hormones such as progesterone consistently were shown to alter hERG distribution by disrupting the homeostasis of cholesterol—the main constituent of caveolae.[35] Whether this process depends upon CAVIN1 remains to be determined.

As per the International Conference on Harmonisation S7B/E14 guidelines, evaluation of the potential of a novel drug to delay cardiac repolarization is specifically addressed in animal and in vitro models, typically heterologous expression systems of ion channels,[36] which, however, are limited by their capacity to recapitulate the complex human cardiac electrophysiology and the interindividual variability to develop cardiotoxic side effe cts.[10,11,37,38] As a consequence, many drugs have escaped preclinical elimination, and some have been ultimately withdrawn from the market.[39,40] The Comprehensive in vitro Proarrhythmia Assay recently added human iPS-CMs to drug safety evaluation.[41] In line with our previous results,[10] here, we show that the cardiotoxic response of iPS-derived cells is variable and depends on the predilection to diLQT, as observed in the patient from whom iPSCs were generated. In addition, this hiPSC platform offers the unique opportunity to test the response to multiple offending drugs, which will not be possible in patients with proven diLQT. We observed for the first time a cross-sensitivity to other drugs targeting hERG (such as vandetanib, E4031, and clarithromycin) that was also dependent on CAVIN1 expression. This observation also suggests that activation of the CAVIN1 system is likely triggered when the hERG channel activity is reduced rather than by a specific binding of drugs to the channel, but this requires further investigation. Altogether, these findings emphasize the potential of using patient-specific iPS-CMs for drug safety screening, modeling of interindividual variability, and identification of molecular culprits.

Our study has some limitations that should be acknowledged. The level of CAVIN1 expression within iPS-derived cardiomyocytes appeared as a critical marker of the susceptibility to develop diLQT. There is no accurate way to estimate CAVIN1 expression in the human myocardium. Additional investigations are warranted to establish the translational value of previous estimation of CAVIN1 expression in candidates to receive a hERG blocker. The acceleration of the channel degradation was described in response to other stimuli such as hypokalemia[23,42,43] or drugs[19,44]; whether CAVIN1 controls these processes is yet to be established.

This study identified a common molecular modulator of the susceptibility to diLQT in human iPS-CMs derived from individuals with different genetic backgrounds. CAVIN1 controlled membranous hERG turnover upon pharmaceutical stimulation, and therefore the repolarization duration. Different expression levels of this marker may explain the interindividual variability in response to hERG blockers. Thus, these results classify CAVIN1 as a potential risk factor for diLQT and open perspectives for a personalized drug prescription to avoid cardiotoxicity.

ARTICLE INFORMATION

Received January 11, 2023; accepted March 21, 2024.

Affiliations

PARCC, INSERM (Z.R.A.S., C.P., C.J., N.M., J.-S.H.), Institut Jacques Monod, CNRS (R.L.B., J.-M.V.), and Ultrastructural BioImaging Core Facility (UBI), C2RT, Institut Pasteur (E.P., A.M.), Université Paris Cité, Paris, France. INSERM U1143, CNRS UMR 3666, PSL Research University, Institut Curie, Paris, France (C.V.d.L., C.L.). Université de Nantes, CNRS, INSERM, l'Institut du Thorax, Nantes, France (G.L.). INSERM UMR_S 1219, Bordeaux Population Health Research Center, University of Bordeaux, France (D.-A.T.). CIC1418 and DMU CARTE, AP-HP, Hôpital Européen Georges-Pompidou, Paris, France (J.-S.H.).

Acknowledgments

The authors thank the Nikon Imaging Centre at Institut Curie-CNRS, member of the French National Research Infrastructure France-BioImaging (ANR10-INSB-04); and ImagoSeine core facility of Institut Jacques Monod, member of France-BioImaging (ANR-10-INBS-04) and IbiSA, with the support of Labex "Who Am I," Inserm Plan Cancer, Region Ile-de-France, and Fondation Bettencourt Schueller.

Sources of Funding

This work was supported by grants from the Foundation Leducq (CVD18-05) and the Fondation pour la Recherche Médicale (EQU201903007852). Dr Lamaze's work was supported by institutional grants from the Curie Institute, Institut National de la Santé et de la Recherche Médicale, and the National Centre for Scientific Research, and specific grants from l'Agence Nationale de la Recherche (ANR-20-CE13-0002-01) and Institut National du Cancer (INCa PL BIO-21-176). Outside the submitted work, Dr Hulot is supported by Assistance

Publique–Hôpitaux de Paris, Institut National de la Santé et de la Recherche Médicale, and l'Agence Nationale de la Recherche, and is coordinating a French PIA Project (2018-PSPC-07, PACIFIC-preserved, BPIFrance) and a University Research Federation Against Heart Failure Project (FHU2019, PREVENT_Heart Failure).

Disclosures

Dr Hulot reports research grants from BioSerenity, Sanofi, Servier, and Novo Nordisk, and speaker, advisory board, or consultancy fees from Amgen, AstraZeneca, Bayer, BioSerenity, Bristol Myers Squibb, Novartis, Novo Nordisk, and Vifor Pharma, all unrelated to the present work. The other authors declare no competing financial interests.

Supplemental Material

Methods
Tables S1–S3
Figures S1–S9

REFERENCES

1. Behr ER, January C, Schulze-Bahr E, Grace AA, Kaab S, Fiszman M, Gathers S, Buckman S, Youssef A, Pirmohamed M, et al. The International Serious Adverse Events Consortium (iSAEC) phenotype standardization project for drug-induced torsades de pointes. *Eur Heart J*. 2013;34:1958–1963. doi: 10.1093/eurheartj/ehs172
2. Mitcheson JS, Chen J, Lin M, Culberson C, Sanguinetti MC. A structural basis for drug-induced long QT syndrome. *Proc Natl Acad Sci U S A*. 2000;97:12329–12333. doi: 10.1073/pnas.210244497
3. Schwartz PJ, Woosley RL. Predicting the unpredictable: drug-induced QT prolongation and torsades de pointes. *J Am Coll Cardiol*. 2016;67:1639–1650. doi: 10.1016/j.jacc.2015.12.063
4. Strauss DG, Vicente J, Johannesen L, Blinova K, Mason JW, Weeke P, Behr ER, Roden DM, Woosley R, Kosova G, et al. Common genetic variant risk score is associated with drug-induced QT prolongation and torsade de pointes risk: a pilot study. *Circulation*. 2017;135:1300–1310. doi: 10.1161/CIRCULATIONAHA.116.023980
5. Fujii Y, Matsumoto Y, Hayashi K, Ding WG, Tomita Y, Fukumoto D, Wada Y, Ichikawa M, Sonoda K, Ozawa J, et al. Contribution of a KCNH2 variant in genotyped long QT syndrome: Romano-Ward syndrome under double mutations and acquired long QT syndrome under heterozygote. *J Cardiol*. 2017;70:74–79. doi: 10.1016/j.jjcc.2016.09.010
6. Kannankeril PJ, Roden DM, Norris KJ, Whalen SP, George AL Jr, Murray KT. Genetic susceptibility to acquired long QT syndrome: pharmacologic challenge in first-degree relatives. *Heart Rhythm*. 2005;2:134–140. doi: 10.1016/j.hrthm.2004.10.039
7. Bellocq C, Wilders R, Schott JJ, Louerat-Oriou B, Boisseau P, Le Marec H, Escande D, Baro I. A common antitussive drug, clobutinol, precipitates the long QT syndrome 2. *Mol Pharmacol*. 2004;66:1093–1102. doi: 10.1124/mol.104.001065
8. Itoh H, Crotti L, Aiba T, Spazzolini C, Denjoy I, Fressart V, Hayashi K, Nakajima T, Ohno S, Makiyama T, et al. The genetics underlying acquired long QT syndrome: impact for genetic screening. *Eur Heart J*. 2016;37:1456–1464. doi: 10.1093/eurheartj/ehv695
9. Salem JE, Germain M, Hulot JS, Voiriot P, Lebourgeois B, Waldura J, Tregouet DA, Charbit B, Funck-Brentano C. Genome-wide Analysis of Sotalol-Induced Ikr Inhibition During Ventricular Repolarization, "GENEREPOL study": lack of common variants with large effect sizes. *PloS One*. 2017;12:e0181875. doi: 10.1371/journal.pone.0181875
10. Stillitano F, Hansen J, Kong CW, Karakikes I, Funck-Brentano C, Geng L, Scott S, Reynier S, Wu M, Valogne Y, et al. Modeling susceptibility to drug-induced long QT with a panel of subject-specific induced pluripotent stem cells. *Elife*. 2017;6:e19406. doi: 10.7554/eLife.19406
11. Shinozawa T, Nakamura K, Shoji M, Morita M, Kimura M, Furukawa H, Ueda H, Shiramoto M, Matsuguma K, Kaji Y, et al. Recapitulation of clinical individual susceptibility to drug-induced QT prolongation in healthy subjects using iPSC-derived cardiomyocytes. *Stem Cell Rep*. 2017;8:226–234. doi: 10.1016/j.stemcr.2016.12.014
12. Al Sayed ZR, Jouni M, Gourraud JB, Belbachir N, Barc J, Girardeau A, Forest V, Derevier A, Gaignerie A, Chariau C, et al. A consistent arrhythmogenic trait in Brugada syndrome cellular phenotype. *Clin Transl Med*. 2021;11:e413. doi: 10.1002/ctm2.413
13. Balijepalli RC, Kamp TJ. Caveolae, ion channels and cardiac arrhythmias. *Prog Biophys Mol Biol*. 2008;98:149–160. doi: 10.1016/j.pbiomolbio.2009.01.012
14. Hill MM, Bastiani M, Luetterforst R, Kirkham M, Kirkham A, Nixon SJ, Walser P, Abankwa D, Oorschot VM, Martin S, et al. PTRF-Cavin, a conserved cytoplasmic protein required for caveola formation and function. *Cell*. 2008;132:113–124. doi: 10.1016/j.cell.2007.11.042
15. Sotodosos-Alonso L, Pulgarin-Alfaro M, Del Pozo MA. Caveolae mechanotransduction at the interface between cytoskeleton and extracellular matrix. *Cells*. 2023;12:942. doi: 10.3390/cells12060942
16. Macia E, Ehrlich M, Massol R, Boucrot E, Brunner C, Kirchhausen T. Dynasore, a cell-permeable inhibitor of dynamin. *Dev Cell*. 2006;10:839–850. doi: 10.1016/j.devcel.2006.04.002
17. Tillu VA, Rae J, Gao Y, Ariotti N, Floetenmeyer M, Kovtun O, McMahon KA, Chaudhary N, Parton RG, Collins BM. Cavin1 intrinsically disordered domains are essential for fuzzy electrostatic interactions and caveola formation. *Nat Commun*. 2021;12:931. doi: 10.1038/s41467-021-21035-4
18. Balijepalli RC, Delisle BP, Balijepalli SY, Foell JD, Slind JK, Kamp TJ, January CT. Kv11.1 (ERG1) K+ channels localize in cholesterol and sphingolipid enriched membranes and are modulated by membrane cholesterol. *Channels (Austin)*. 2007;1:263–272. doi: 10.4161/chan.4946
19. Guo J, Li X, Shallow H, Xu J, Yang T, Massaeli H, Li W, Sun T, Pierce GN, Zhang S. Involvement of caveolin in probucol-induced reduction in hERG plasma-membrane expression. *Mol Pharmacol*. 2011;79:806–813. doi: 10.1124/mol.110.069419
20. Rajab A, Straub V, McCann LJ, Seelow D, Varon R, Barresi R, Schulze A, Lucke B, Lutzkendorf S, Karbasiyan M, et al. Fatal cardiac arrhythmia and long-QT syndrome in a new form of congenital generalized lipodystrophy with muscle rippling (CGL4) due to PTRF-CAVIN mutations. *PloS Genet*. 2010;6:e1000874. doi: 10.1371/journal.pgen.1000874
21. Taniguchi T, Maruyama N, Ogata T, Kasahara T, Nakanishi N, Miyagawa K, Naito D, Hamaoka T, Nishi M, Matoba S, et al. PTRF/Cavin-1 deficiency causes cardiac dysfunction accompanied by cardiomyocyte hypertrophy and cardiac fibrosis. *PloS One*. 2016;11:e0162513. doi: 10.1371/journal.pone.0162513
22. Hedley PL, Kanters JK, Dembic M, Jespersen T, Skibsbye L, Aidt FH, Eschen O, Graff C, Behr ER, Schlamowitz S, et al. The role of CAV3 in long-QT syndrome: clinical and functional assessment of a caveolin-3/Kv11.1 double heterozygote versus caveolin-3 single heterozygote. *Circ Cardiovasc Genet*. 2013;6:452–461. doi: 10.1161/CIRCGENETICS.113.000137
23. Massaeli H, Sun T, Li X, Shallow H, Wu J, Xu J, Li W, Hanson C, Guo J, Zhang S. Involvement of caveolin in low K+-induced endocytic degradation of cell-surface human ether-a-go-go-related gene (hERG) channels. *J Biol Chem*. 2010;285:27259–27264. doi: 10.1074/jbc.M110.124909
24. Guo J, Wang T, Li X, Shallow H, Yang T, Li W, Xu J, Fridman MD, Yang X, Zhang S. Cell surface expression of human ether-a-go-go-related gene (hERG) channels is regulated by caveolin-3 protein via the ubiquitin ligase Nedd4-2. *J Biol Chem*. 2012;287:33132–33141. doi: 10.1074/jbc.M112.389643
25. Cherubini A, Hofmann G, Pillozzi S, Guasti L, Crociani O, Cilia E, Di Stefano P, Degani S, Balzi M, Olivotto M, et al. Human ether-a-go-go-related gene 1 channels are physically linked to beta1 integrins and modulate adhesion-dependent signaling. *Mol Biol Cell*. 2005;16:2972–2983. doi: 10.1091/mbc.e04-10-0940
26. Goldenring JR. A central role for vesicle trafficking in epithelial neoplasia: intracellular highways to carcinogenesis. *Nat Rev Cancer*. 2013;13:813–820. doi: 10.1038/nrc3601
27. Lamothe SM, Guo J, Li W, Yang T, Zhang S. The human ether-a-go-go-related gene (hERG) potassium channel represents an unusual target for protease-mediated damage. *J Biol Chem*. 2016;291:20387–20401. doi: 10.1074/jbc.M116.743138
28. Guo J, Wang T, Yang T, Xu J, Li W, Fridman MD, Fisher JT, Zhang S. Interaction between the cardiac rapidly (Ikr) and slowly (Iks) activating delayed rectifier potassium channels revealed by low K+-induced hERG endocytic degradation. *J Biol Chem*. 2011;286:34664–34674. doi: 10.1074/jbc.M111.253351
29. Rajamani S, Anderson CL, Valdivia CR, Eckhardt LL, Foell JD, Robertson GA, Kamp TJ, Makielski JC, Anson BD, January CT. Specific serine proteases selectively damage KCNH2 (hERG1) potassium channels and I(Kr). *Am J Physiol Heart Circ Physiol*. 2006;290:H1278–H1288. doi: 10.1152/ajpheart.00777.2005
30. Chen J, Guo J, Yang T, Li W, Lamothe SM, Kang Y, Szendrey JA, Zhang S. Rab11-dependent Recycling of the human ether-a-go-go-related gene (hERG) channel. *J Biol Chem*. 2015;290:21101–21113. doi: 10.1074/jbc.M115.636324
31. Delisle BP, Underkofler HAS, Moungey BM, Slind JK, Kilby JA, Best JM, Foell JD, Balijepalli RC, Kamp TJ, January CT. Small GTPase determinants for the Golgi processing and plasmalemmal expression of human

ether-a-go-go related (hERG) K+ channels. *J Biol Chem*. 2009;284:2844–2853. doi: 10.1074/jbc.M807289200
32. Sangoi MG, Lamothe SM, Guo J, Yang T, Li W, Avery EG, Fisher JT, Zhang S. Beta-Arrestin-mediated regulation of the human ether-a-go-go-related gene potassium channel. *Mol Pharmacol*. 2017;92:162–174. doi: 10.1124/mol.116.108035
33. Lamothe SM, Zhang S. The serum- and glucocorticoid-inducible kinases SGK1 and SGK3 regulate hERG channel expression via ubiquitin ligase Nedd4-2 and GTPase Rab11. *J Biol Chem*. 2013;288:15075–15084. doi: 10.1074/jbc.M113.453670
34. Salem JE, Dureau P, Bachelot A, Germain M, Voiriot P, Lebourgeois B, Tregouet DA, Hulot JS, Funck-Brentano C. Association of oral contraceptives with drug-induced QT interval prolongation in healthy nonmenopausal women. *JAMA Cardiol*. 2018;3:877–882. doi: 10.1001/jamacardio.2018.2251
35. Wu ZY, Yu DJ, Soong TW, Dawe GS, Bian JS. Progesterone impairs human ether-a-go-go-related gene (HERG) trafficking by disruption of intracellular cholesterol homeostasis. *J Biol Chem*. 2011;286:22186–22194. doi: 10.1074/jbc.M110.198853
36. US Food and Drug Administration. S7B nonclinical evaluation of the potential for delayed ventricular repolarization (QT interval prolongation) by human pharmaceuticals. Published October 2005. https://www.fda.gov/regulatory-information/search-fda-guidance-documents/s7b-nonclinical-evaluation-potential-delayed-ventricular-repolarization-qt-interval-prolongation
37. Weeke P, Delaney J, Mosley JD, Wells Q, Van Driest S, Norris K, Kucera G, Stubblefield T, Roden DM. QT variability during initial exposure to sotalol: experience based on a large electronic medical record. *Europace*. 2013;15:1791–1797. doi: 10.1093/europace/eut153
38. Baracaldo-Santamaria D, Llinas-Caballero K, Corso-Ramirez JM, Restrepo CM, Dominguez-Dominguez CA, Fonseca-Mendoza DJ, Calderon-Ospina CA. Genetic and molecular aspects of drug-induced QT interval prolongation. *Int J Mol Sci*. 2021;22:8090. doi: 10.3390/ijms22158090
39. Onakpoya IJ, Heneghan CJ, Aronson JK. Post-marketing withdrawal of 462 medicinal products because of adverse drug reactions: a systematic review of the world literature. *BMC Med*. 2016;14:10. doi: 10.1186/s12916-016-0553-2
40. Antoniou CK, Dilaveris P, Manolakou P, Galanakos S, Magkas N, Gatzoulis K, Tousoulis D. QT prolongation and malignant arrhythmia: how serious a problem? *Eur Cardiol*. 2017;12:112–120. doi: 10.15420/ecr.2017:16:1
41. Gintant G, Fermini B, Stockbridge N, Strauss D. The evolving roles of human iPSC-derived cardiomyocytes in drug safety and discovery. *Cell Stem Cell*. 2017;21:14–17. doi: 10.1016/j.stem.2017.06.005
42. Guo J, Massaeli H, Xu J, Jia Z, Wigle JT, Mesaeli N, Zhang S. Extracellular K+ concentration controls cell surface density of Ikr in rabbit hearts and of the HERG channel in human cell lines. *J Clin Invest*. 2009;119:2745–2757. doi: 10.1172/JCI39027
43. Massaeli H, Guo J, Xu J, Zhang S. Extracellular K+ is a prerequisite for the function and plasma membrane stability of HERG channels. *Circ Res*. 2010;106:1072–1082. doi: 10.1161/CIRCRESAHA.109.215970
44. Dennis AT, Nassal D, Deschenes I, Thomas D, Ficker E. Antidepressant-induced ubiquitination and degradation of the cardiac potassium channel hERG. *J Biol Chem*. 2011;286:34413–34425. doi: 10.1074/jbc.M111.254367